CHARACTERIZATION OF A SEPARATED TURBULENT BOUNDARY LAYER FOR FLOW CONTROL PURPOSE.

C. Cuvier[1,2], **C. Braud**[1,3], **J.M. Foucaut**[1,2], **M. Stanislas**[1,2]
Univ Lille Nord de France[1] F-59000 Lille, EC Lille[2], CNRS[3],
Laboratoire de Mécanique de Lille (UMR 8107)
Boulevard Paul Langevin,
59655 Villeneuve d'Ascq Cédex, France.
christophe.cuvier@gmail.com
caroline.braud@univ-lille1.fr
jean-marc.foucaut@ec-lille.fr
michel.stanislas@ec-lille.fr

ABSTRACT

The flow over a two dimensional ramp has been characterized. First, some configurations of the ramp were characterized rapidly with only wall pressure measurements and wool tufts visualisations. The aim of this first work was to check the spanwise homogeneity and to find the angle α and β of the ramp that give a ramp configuration with an adverse pressure gradient on the 2 m flat plate and a separation on the flap. It was found that for $\alpha = -2^\circ$, the separation occur on the flap for β under -19°. The configuration with $\alpha = -2^\circ$ and $\beta = -22^\circ$ was then selected and characterized more carefully with hot-wire profiles. On this configuration, the boundary layer over the ramp is around 20 cm and the Reynolds number based on the momentum thickness (Re_θ) is around 11 000. The boundary layer under study develops with a mild adverse pressure gradient with a Clauser pressure parameter between 0.2 and 1.4. At the end of the 2 m flat plate of the ramp, there is a separation on the flap which is more or less two dimensional on 70 % of the span. This flow mimics the suction side of a wing and is then adapted to do parametric studies of flow control.

Key words : Turbulent boundary layers, adverse pressure gradient, hot-wire, flow separation.

INTRODUCTION

Turbulent Boundary Layer (TBL) that encountered adverse pressure gradient (APG) seems to be inevitable in turbomachinery and aircraft applications. Sometimes, the APG encountered is strong enough to lead to a flow separation. The flow detachment has drastic consequences on the efficiency of turbo-machineries and can lead to a loss of control of an aircraft. The studies of a boundary layer in adverse pressure gradient with separation is thus interesting for industrial applications. It is not surprising that recently many experimental (Webster et al., 1996; Bernard et al., 2003; Aubertine and Eaton, 2005; Elsberry et al., 2000; Angele and Muhammad-Klingmann, 2006; etc.) and numerical (Wu and Squires, 1998; etc.) studies have appeared on APG boundary layers.

From the experimental point of view, there are three major ways to generate and study the boundary layers in adverse pressure gradient. The first one is a wind tunnel with a flexible wall that allows the diverging cross section to be tuned in order to fix the pressure gradient (like in Elsberry et al., 2000; Angele and Muhammad-Klingmann, 2006). The second one is a bump shaped model sets in the test section of a wind tunnel (like in Webster et al., 1996; Bernard et al., 2003). The last one is very closed to a bump. it corresponds to a ramp (like in Aubertine and Eaton, 2005). Bump and ramp have to be distinguished because the boundary layer over a bump is influenced by both adverse pressure gradient and surface curvature effects. In some flow, it was shown that surface curvature can have more effects on the turbulent quantities than the adverse pressure gradient (Talapurkara et al., 2001). The three major ways of generating adverse pressure gradient give a huge numbers of different experiments, which differ also from one another by the strength of the adverse pressure gradient that can lead or not to a flow separation.

The scaling of the mean velocity profile and the turbulent shear stress seems to be not yet fixed. For the inner region near to the wall, it seems to be accepted that the velocity scale is the friction velocity ($u_\tau = \sqrt{\frac{\tau_w}{\rho}}$, where τ_w is the friction at the wall) and the length scale is $\frac{\nu}{u_\tau}$ (George, 2005). For the outer part it is more controversial. The first theory for the scaling of the outer part was the Clauser one (Clauser, 1954). It this theory, the proposed velocity scale of the outer part was u_τ and the proposed length scale was δ, the boundary layer thickness. In that theory, the profiles have to collapse by plotting $\frac{U_e - U}{u_\tau} = f(\frac{y}{\delta})$, with U_e the free-stream velocity. By merging the outer law and the inner law, the log-law is obtained. As the Clauser's theory was not fully satisfactory, new theories, based on similarity analysis, have appeared for boundary layers in APG. Castillo and George (2001), for infinite Reynolds number boundary layers, proposed U_e for the velocity scale

in the outer part. If their theory is right, the profiles would collapse by plotting $\frac{U_e-U}{U_e} = f(\frac{y}{\delta})$. However, it seems to be not really the case. Zagarola and Smits (1998) have propose $U_e \frac{\delta^*}{\delta}$ as outer velocity scales. This representation seems to work quite well in many experiments. Maciel et al. (2006) explain that the Zagarola outer velocity scale gives a Reynolds number correction to the similarity analysis of Castillo and George (2001). It seems to appear that the inner velocity scale is different from the outer velocity scale. According to George (2005), the different velocity scales for the inner and the outer layer lead to the impossibility of a log layer. This discredit the estimation done by many authors of the friction velocity u_τ by fitting a log-law on the mean velocity profile as suggested by Clauser (1956).

The experiment presented here is a two dimensional ramp-type, designed for the AVERT (Aerodynamic Validation of Emission Reducing Technologies) FP6 EC project, with a mild adverse pressure gradient on a 2 m flat plate. At the end of the flat plate, there is an imposed separation on a flap. This flow is well adapted to a detail study of flow separation control as it mimics the flow on the suction side of a wing.

THE EXPERIMENT

The wind tunnel facility and the ramp

The experiment was conducted in the LML boundary layer wind tunnel at $U_\infty = 10$ m/s. A boundary layer develops on the 20 m long lower wall to reach around 30 cm at the end. This thick boundary layer allows good spatial resolution of the measurements. The test section is 2 m span and 1 m height and the free-stream velocity is ranging from 1 to 10 m/s ($\pm 0.5\%$). In this experiment, the wind tunnel was used in close-loop configuration with temperature regulation ($\pm 0.2°C$). For details characteristics of the wind tunnel, see Carlier and Stanislas (2005).

The ramp model was mounted on the wind tunnel floor such as the beginning of the ramp was 14.4 m downstream of the entrance of the test section. Figure 1 gives a schematic view of the ramp. It is composed of four parts. The first one is a smooth converging part with a contraction ratio of 0.75 to allow to generate a pressure gradient flow after it. At the beginning of the converging part, suction (not used in the present experiment) can be applied to tune the incoming boundary layer. The second part is an articulated flat plate of more than 2 m. The angle between this plate and the wind tunnel floor is called α and is counted positive if it corresponds to a positive rotation around the z axis (Figure 1). The angle α tunes the pressure gradient of the boundary layer that develops on the 2.1 m flat plate. α is ranging from $2°$ to $-4°$. The third part of the ramp is an other articulated flat plate (called flap). The angle between this plate and the wind tunnel floor is called β and its sign used the same convention as α. β is ranging from $-5°$ to $-40°$. The aim of the flap is to allow to create and fix a flow separation. The angle β tunes the strength and the extend of the flow separation. The last part is a flexible plate to allow smooth connection between the end of the flap and the floor of the wind tunnel.

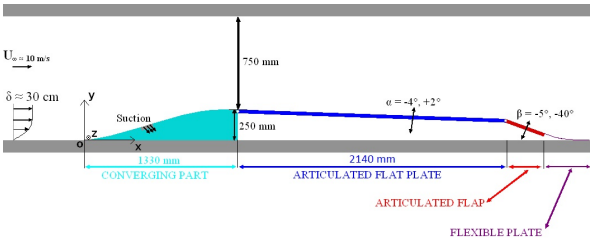

Figure 1. Schematic view of the ramp.

Experimental techniques

Different measurement techniques were used to characterize the flow over the ramp.

Wool tufts and oil film visualisations Wool tufts visualisations was performed on the flat plate and on the flap to characterize the two dimensional behaviour of the flow over the ramp. They were also used to evidence flow separation. Several lines of wool tufts of 4 cm long were placed on the flat plate on all the span. On the flap, a larger density of wool tufts was applied because flow separation was expected on it. In the case with an adverse pressure gradient on the flat plate and a separation on the flap ($\alpha = -2°$ and $\beta = -22°$), oil film visualisation was applied on the flap to characterized the two dimensional behaviour of the separation. The mixture used was composed of paraffin oil (82%), oleic acid (9%) and titanium dioxide (9%).

Pressure measurements Wall pressure measurements were used to characterize the pressure distribution on the ramp for different angles α and β ($-2° \leq \alpha \leq 0°$ and $-22° \leq \beta \leq -6°$). The pressure taps are 0.5 mm in diameter. They were connected with a manual scanivalve and read with a Furness micro-manometer differential sensor (reference FC014, range: 0 to 10 mmH_2O, accuracy : $\pm 0.5\%$ of the measured value in the range 0.01 to 10 mmH_2O). The pressure coefficient C_p ($C_p = \frac{P-P_6}{\frac{1}{2}\rho U_\infty^2}$) was calculated with pressure tap number 6 as reference (i.e. the last in the converging part). The uncertainty is estimated to be $\pm 1.3\%$ for C_p and $\pm 6\%$ for $\frac{dC_p}{ds}$. More details about these uncertainty estimations can be found in Cuvier et al. (2010).

Single hot-wire measurements Single hot-wire measurements were performed on the configuration with $\alpha = -2°$ and $\beta = -22°$ to assess the boundary layer characteristics. The anemometer used was a constant temperature AN 1003 manufactured by AAlabSystems with a boundary layer type hot-wire with a diameter of 2.5 μm and a length of 0.5 mm. The length of the wire used is about 15 wall units, that is slightly too large for highly accurate measurements of turbulent intensity compared to the value recommended by Klewicki and Falco (1990). The calibration of the wire was done in situ at mid height of the wind-tunnel. A pitot tube was set at the same place, separated by 20 cm in span to measure the speed. A King's law was used for the calibration. Each profile is composed of 49 points distributed logarithmically along the wall normal. The first point is about 0.2 mm

from the wall and was measured with a cathetometer at ± 0.05 mm. Based on the study of Carlier and Stanislas (2005), the acquisition frequency was 11 kHz and the cut off frequency was 5 kHz. 1.1 million samples were taken for the first 30 points, 2.2 million for the 14 following, and 4.4 million for the last points. The estimated uncertainty on the mean velocity is about $\pm 1\%$, on the turbulent intensity $\pm 2.8\%$, on the third order moment $\pm 7.2\%$ and on the four order moment $\pm 5.2\%$. More details about these uncertainty estimations can be found in Cuvier et al. (2010).

RESULTS AND DISCUSSION

The wool tufts visualisations, for all the angles α and β tested, have shown that there is no separation on the flat plate. End effects appear near the side walls and grow near the flap to reach 10 cm at the flap articulation when $\alpha = -2^\circ$ and $\beta = -22^\circ$. By combining the results of wool tufts visualisations and spanwise pressure distribution at two stations on the flat plate, it appears that the flow remains two dimensional in the mean over more than 90% of the span. Separation occurs on the flap for β under -19° and $\alpha = -2^\circ$. The end effects are larger on the flap (about 30 cm) due to a stronger pressure gradient. The spanwise homogeneity of the separation was checked by oil film visualisation ($\alpha = -2^\circ$ and $\beta = -22^\circ$). It results that the separation on the flap remains more or less 2D on 70% (i.e. 1400 mm) of the span of the flap and it is fixed at the flap articulation.

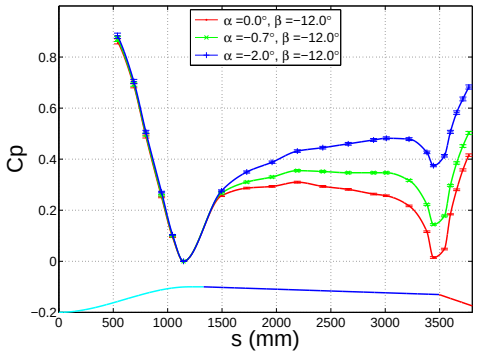

Figure 2. Streamwise pressure coefficient distribution, for different α, $\beta = -12^\circ$ and $U_\infty = 10$ m/s.

Figures 2 and 3 give the pressure coefficient distribution and the pressure gradient distribution for different angles α and $\beta = -12^\circ$. The flow accelerates in the converging part $0 \leq s \leq 1360$ mm (s is the curvilinear coordinate along the ramp) which induces a decrease of the pressure coefficient until the suction peak at $s = 1146$ mm (pressure tap number 6). Then a pressure recovery occurs on the flat plate which is modified by α. At the flap articulation, a new suction peak occurs which can be seen at $s = 3443$ mm corresponding to pressure tap 17. Then a pressure recovery is observed on the flap which can be tuned by β. In the middle of the flat plate, the pressure gradient is almost constant (Figure 3), and a zero pressure gradient is obtained in this 60 cm long area

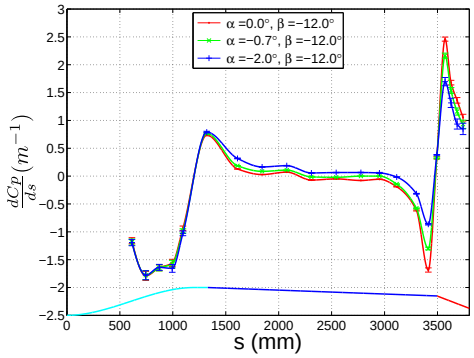

Figure 3. Streamwise pressure gradient distribution, for different α, $\beta = -12^\circ$ and $U_\infty = 10$ m/s.

for $\alpha = -0.7^\circ$, a favourable for $\alpha > -0.7^\circ$ and an adverse for $\alpha < -0.7^\circ$. It was checked that there is no influence of the parameter β on the pressure gradient on the flat plate until $s = 3010$ mm or pressure tap number 14. Figure 4 gives the pressure gradient distribution for $\alpha = -2^\circ$ and $\beta = -22^\circ$, which corresponds to the ramp configuration where the hot-wire profiles were obtained.

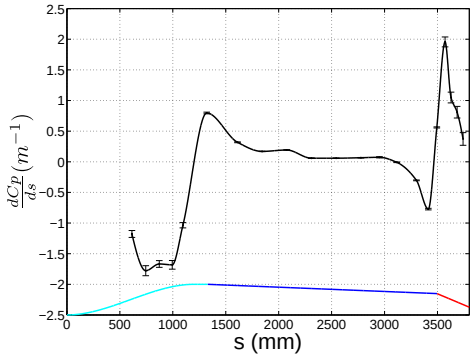

Figure 4. Streamwise pressure gradient distribution, for $\alpha = -2^\circ$, $\beta = -22^\circ$ and $U_\infty = 10$ m/s.

Figure 5 gives the positions on the ramp of the five hot-wire profiles that were carried out on the configuration with $\alpha = -2^\circ$, $\beta = -22^\circ$ and $U_\infty = 10$ m/s. Each profile was repeated several times in order to obtained three coherent profiles that superimposed better than 2%. The boundary layer parameters are given in Table 1. The Reynolds number based on the momentum thickness is of the order of 11 000, that is about the Reynolds number of the LML wind tunnel in flat plate (FP) configuration at 5 m/s. The near wall region of all the profiles obtained can thus be compared to this FP configuration.

The boundary layer thickness δ begins at 17.4 cm at station 1 and grows with s and with the adverse pressure gradient to reach 21.2 cm at station 4. Between stations 4 and 5, the boundary layer thickness decreases as the suction peak in this area introduces favourable pressure gradient. The shape factor H follows the same behaviour as δ. It begins at 1.18 at

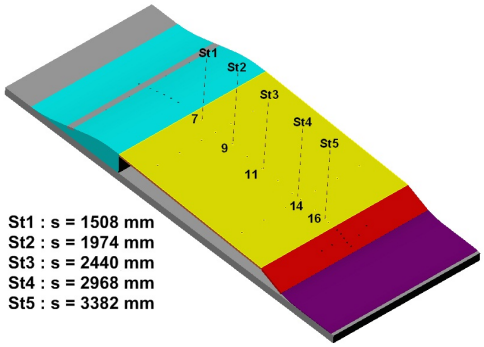

Figure 5. Location of the hot-wire profiles.

Table 1. Boundary layer characteristics at $U_\infty = 10$ m/s, $\alpha = -2°$, $\beta = -22°$.

St	s (mm)	δ (cm)	δ^* (mm)	θ (mm)	Re_θ
St1	1508	17.4	14.4	12.2	10100
St2	1974	19.6	16.5	13.7	10600
St3	2440	20.3	17.9	14.7	11700
St4	2968	21.2	20.3	16.5	12600
St5	3382	19.0	16.4	13.5	10100

St	H	U_e (m/s)	u_τ (m/s)	$(\frac{\partial P}{\partial s})^+$ ($\times 10^3$)	$\beta_{Clauser}$
St1	1.18	12.9	0.482	3.28	1.44
St2	1.21	12.6	0.459	1.47	0.70
St3	1.22	12.5	0.462	0.46	0.24
St4	1.23	12.4	0.435	0.67	0.38
St5	1.21	12.3	0.465	-5.54	-2.56

station 1. This value is coherent with the shape factor of the incoming boundary layer (1.3) on the ramp as it is decreased in the converging part where favourable pressure gradient is encountered.

The friction velocity was determined by fitting equation (1) on the mean velocity profile (Bernard et al., 2003) in adverse pressure gradient (stations 1 to 4) and a log-law in favourable pressure gradient (station 5). Equation (1) is obtained by integrating the inner boundary layer equation and by supposing that the mixing length theory remains valid for adverse pressure gradient boundary layer. The constant of integration C2 is obtained by identifying equation (1) with the standard log-law as the term $(\frac{\partial P}{\partial x})^+ y^+$ becomes small compare to 1. C2 is given by equation (2). κ was taken as 0.41 and C as 5.0. The advantage of this equation compare to the log-law is that it presents a curvature that follows better the mean velocity profile. To optimize the fit, the value y_0 of the first point was adjusted in its uncertainty interval.

$$U^+ = \frac{1}{\kappa}(2\sqrt{1+(\frac{\partial P}{\partial x})^+ y^+} + \ln|\sqrt{1+(\frac{\partial P}{\partial x})^+ y^+} - 1| - \ln(\sqrt{1+(\frac{\partial P}{\partial x})^+ y^+} + 1)) + C2 \quad (1)$$

$$C2 = -\frac{1}{\kappa}(2 - \ln(2) + \ln\frac{1}{2}|(\frac{\partial P}{\partial x})^+|) + C \quad (2)$$

The uncertainty on δ is about $\pm 10\%$, and on δ^*, θ and u_τ about $\pm 5\%$. The uncertainty on U_e is $\pm 0.6\%$. The uncertainties on the pressure parameters are then higher of about $\pm 20\%$ due mostly to the uncertainty on the pressure gradient and on u_τ.

As was introduce by Castillo and George (2001), the boundary layer is in equilibrium state if the free-stream velocity is proportional to the boundary layer thickness at power $-\Lambda$ with $\Lambda = \frac{\delta}{\rho U_e^2 \frac{d\delta}{dx}} \frac{dP}{dx}$. This was checked for the first four stations that are in adverse pressure gradient. $\ln(U_e)$ versus $\ln(\delta)$ is almost linear with $\Lambda = 0.2$, close to the value of 0.22 observed by these authors for adverse pressure gradient. The boundary layer seems then to be in an equilibrium state as defined by Castillo and George (2001), for the first four stations.

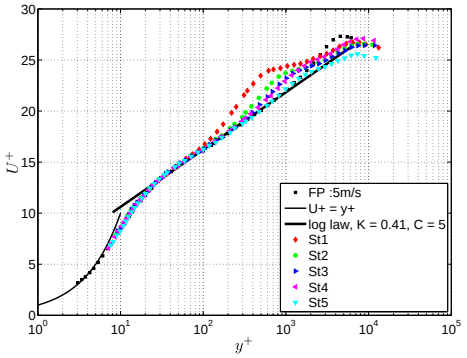

Figure 6. Mean velocity profiles, $\alpha = -2°$, $\beta = -22°$ and $U_\infty = 10$ m/s.

Figure 6 shows the five mean velocity profiles obtained along the ramp in wall units and compared to the FP at 5 m/s. The profiles begin at $y^+ = 9$ for stations 1 to 3, and at $y^+ = 7.5$ for stations 4 and 5 (corresponding to $y \simeq 0.2$ mm). For the three first stations, the probe was not approached nearer to the wall as vibrations were observed and measured by an acceleration sensor stuck on the wall. The displacement was obtained by integrating twice the output of the acceleration sensor. Samples of 10 s were acquired for each station at 11 kHz with a cut-off frequency at 5 kHz to allow to compute spectrum and statistics. The amplitude (estimated by 2σ, with σ the standard deviation) of these vibrations is about 0.5 wall units for stations 1 and 5, and 2 wall units for stations 2 to 4. As these vibrations have an amplitude less than two wall units and their frequencies are small (under 20 Hz), the flow is not affected.

All the profiles collapse for $8 \leq y^+ \leq 100$. This is coherent with the theory as the Reynolds number is almost the same and the pressure gradient is negligible in this region (In equation (1), the term $(\frac{\partial P}{\partial x})^+ y^+$ is smaller than 0.1 for the five stations so negligible compared to 1). The log region extension increases by the decrease of the strength of the adverse pressure gradient from stations 1 to 4. This is not surprising as the shrink of the log region with the strength of the adverse pressure gradient has also been observed by other authors (Aubertine and Eaton, 2005; Bernard et al., 2003;...). After $y^+ > 2000$, the profiles of stations 1 to 4 seem to collapse. This lets supposing that u_τ can be the appropriate external velocity scale. This contradicts the theory of Castillo

and George (2001).

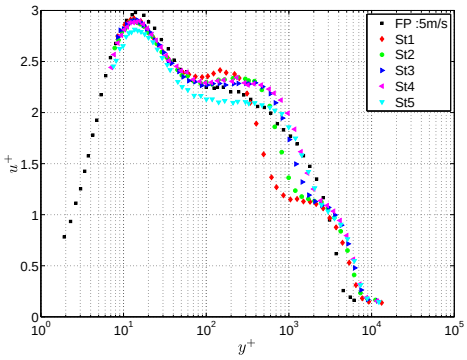

Figure 7. Turbulent intensity profiles, $\alpha = -2°$, $\beta = -22°$ and $U_\infty = 10$ m/s.

Figure 7 shows the evolution of the turbulence intensity profile along the ramp in wall units. The y^+ axis is logarithmic to show in the same plot the near wall region and the region away from the wall. Except for station 5 and FP, all the profiles collapse for $8 \leq y^+ \leq 40$. A first peak of turbulence is observed for all the profiles at $y^+ \simeq 14$ which is characteristic of near wall turbulence. This peak has a value of 2.9 which is slightly smaller than the FP case. This can be attributed to the averaging over the length of the hot-wire (Klewicki and Falco, 1990). The value is smaller at station 5 because the pressure gradient is favourable at this station and tends to attenuate turbulence.

A second peak is observed at the first four stations, around $y^+ \simeq 150$ at station 1, and moving away from the wall with s, to reach $y^+ \simeq 350$ at station 4. This peak is replaced by a plateau at station 5 and for the FP case. This second peak is accompanied with a knee point at $y^+ \simeq 2000$ for the first four stations. The second peak and the knee point were also observed by Webster et al. (1996), Wu and Squires (1998), Baskaran et al. (1987), etc.. The knee point is attributed by Webster et al. (1996) to a proof that a new internal layer near the wall has been triggered in the converging part by the change in curvature. The second peak on the profiles is then attributed to a remnant of the upstream internal layer.

Here, this interpretation is questionable as the knee point seems to stay at the same position. This knee point seems more related to the external turbulence intensity of the incoming boundary layer that has been seriously attenuated by the favourable pressure gradient encounter in the converging part. The second peak in the turbulence intensity profiles is then interpreted as an instability triggered by the change of sign of the pressure gradient near pressure tap 6. This is more coherent because the pressure gradient effects becomes non-negligible in the equations after $y^+ \simeq 100$ in the present study, that is near the position of the second turbulence peak at station 1. The first turbulence peak is not attenuated in the converging part as the pressure gradient effects is small in the near wall region. This first peak is then only governed by the shear due to the wall. This explain why it scale in wall units. In Webster et al. (1996) study, the same explanations on the turbulence intensity profiles seems to apply as it seems that the first turbulence peak that they found scales with wall units. However, contrary to the present study, they found that the first peak position moves away from the wall with the streamwise position. This differences in conclusion can be explain by the difference in the strength of their pressure gradient (compared to the present study, their pressure gradient $\frac{\partial P}{\partial x}^+$ is ten time larger).

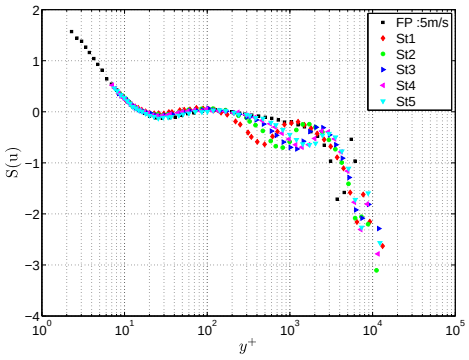

Figure 8. Skewness profiles, $\alpha = -2°$, $\beta = -22°$ and $U_\infty = 10$ m/s.

Figure 8 shows the skewness profiles for the five stations in wall units compared to the FP case. All profiles superimpose with the FP case below $y^+ \simeq 200$. The skewness decreases with y^+ to reach zero at $y^+ \simeq 14$. After it stays constant near zero in the logarithmic region and decreases in the wake region. Contrary to the FP case, it shows a minimum at $y^+ \simeq 500$ for station 1, which moves away from the wall to $y^+ \simeq 1700$ at station 5. After this minimum, all the profiles superimpose with the FP case. The positive values of the skewness under $y^+ \simeq 14$ are the result of wall intermittency (low and high speed streaks, ejections and sweeps). The negative values of the skewness in the wake region are the result of external intermittency. The minimum of skewness near $y^+ \simeq 500$ to 1700 is clearly related again to the instability triggered near pressure tap 6.

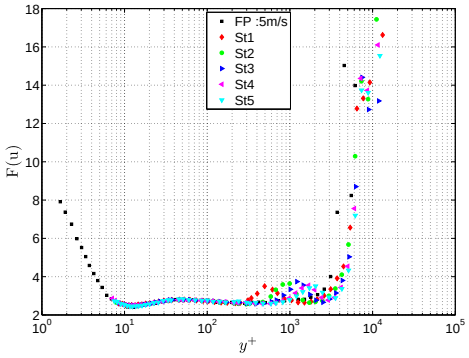

Figure 9. Flatness profiles, $\alpha = -2°$, $\beta = -22°$ and $U_\infty = 10$ m/s.

Figure 9 shows the flatness profiles for the five stations in wall units compared to the FP case. All the profiles superimpose for $y^+ \leq 300$. The flatness decreases from the wall with y^+, to reach a minimum at $y^+ \simeq 14$. Then it slightly increases to reach a value around 2.6 - 2.7 in the logarithmic region. After, the flatness profiles for the five stations differ from the FP case. Indeed, a peak appears around $y^+ \simeq 500$ for station 1, which moves away from the wall with s to reach $y^+ \simeq 2000$ at station 5. This peak is clearly related again to the instability triggered near pressure tap 6. After this second peak, the flatness increases strongly at all five stations, due to intermittency, and superimpose with the FP case.

CONCLUSIONS

The flow characterisation of a two dimensional ramp is presented. Zero, favourable and adverse pressure gradients can be obtained on the flat plate at respectively $\alpha = -0.7°$, $\alpha > -0.7°$ and $\alpha < -0.7°$. A separation occurs on the flap for $\beta = -19°$ and $\alpha = -2°$. The flap adverse pressure gradient tuned by β has no significant effects on the flat plate pressure distribution fixed by α, except on the suction peak just before the flap articulation. The amplitude of this suction peak is characteristic of the separation.

A configuration of the ramp with a mild adverse pressure gradient on the flat plate and a flow separation on the flap is obtained for $\alpha = -2°$, $\beta = -22°$ and $U_\infty = 10$ m/s. This configuration has been characterized more precisely with single hot-wire anemometry. It appears that the boundary layer thickness is around 20 cm, the shape factor is around 1.2 and the Reynolds number based on θ is about 11 000 and is of the same order as for the FP case at $U_\infty = 5$ m/s. The mean velocity profiles exhibit a log region that shrinks with the adverse pressure gradient strength. The existence of a log region was used to estimate the value of the friction velocity with a modified log-law (equation (1)).

The turbulent intensity profiles obtained present two peaks, one near $y^+ = 14$ and one near $y^+ = 150$ at station 1. This second peak moves away from the wall with s. The first peak is attributed to standard near wall turbulence as its scales in wall units. The second one is attributed to an instability triggered by the change of sign of the pressure gradient in the converging part near pressure tap 6. The knee-point in all the turbulence profiles at $y^+ \simeq 2000$ is attributed to a remnant of the external turbulence intensity of the incoming boundary layer that has been seriously attenuated by the favourable pressure gradient encountered in the converging part.

On the skewness and flatness profiles, a local extremum is observed near $y^+ = 500$ at station 1 that moved away from the wall with s. This local extremum is also attributed to the instability triggered by the change of sign of the pressure gradient in the converging part near pressure tap 6.

ACKNOWLEDGEMENTS

The authors would like to thank the European Communauty for their financial support under the contract AVERT/RTD REG/H.3(2006)A/142121. The International Campus on Safety and Intermodality in Transportation (CISIT) is also acknowledge for their financial support.

REFERENCES

Angele, K. P. and Muhammad-Klingmann, B. (2006). Piv measurements in a weakly separating and reattaching turbulent boundary layer. *European Journal of Mechanics B/Fluids*, 25:204–222.

Aubertine, C. D. and Eaton, J. K. (2005). Turbulence development in a non-equilibrium turbulent boundary layer with mild adverse pressure gradient. *Journal of Fluid Mechanics*, 532:345–364.

Baskaran, V., Smits, A. J., and Joubert (1987). A turbulent flow over a curved hill. part 1. growth of an internal boundary layer. *Journal of Fluid Mechanics*, 182:47–83.

Bernard, A., Foucaut, J. M., Dupont, P., and Stanislas, M. (2003). Decelerating boundary layer: A new scaling and mixing length model. *AIAA Journal*, 41(2):248–255.

Carlier, J. and Stanislas, M. (2005). Experimental study of eddy structures in a turbulent boundary layer using particule image velocimetry. *Journal of Fluid Mechanics*, 535(36):143–188.

Castillo, L. and George, W. K. (2001). Similarity analysis for boundary layer with pressure gradient : outer flow. *AIAA journal*, 39(1):41–47.

Clauser, F. H. (1954). The turbulent boundary layer in adverse pressure gradient. *Journal of the aeronautical sciences*, 21:91–108.

Clauser, F. H. (1956). The turbulent boundary layer. *Adv Appl Mech*, 4:1–51.

Cuvier, C., Braud, C., Foucaut, J., and Stanislas, M. (2010). Flow characterisation and parametric study of passive and active vortex generators on the lml-avert ramp. Technical report, AVERT.

Elsberry, K., Loeffler, J., Zhou, M. D., and Wygnanski, I. (2000). An experimental study of a boundary layer that is maintained on the verge of separation. *Journal of Fluid Mechanics*, 423:227–261.

George, W. K. (2005). Recent advancements toward the understanding of turbulent boundary layers. *4th AIAA Theoretical Fluid Mechanics Meeting, 6 - 9 June, Toronto, Canada*, (4669).

Klewicki, J. C. and Falco, R. E. (1990). On accurately measuring statistics associated with small-scales structure in turbulent boundary layers using hot-wire probes. *Journal of Fluid Mechanics*, 219:119–142.

Maciel, Y., Rossignol, K. S., and Lemay, J. (2006). Self-similarity in the outer region of adverse pressure gradient boundary layers. *AIAA paper*, 44:2450–2464.

Talapurkara, E. G., Khosnevis, A. B., and Narasimhan, J. L. (2001). Wake-boundary layer interaction subject to convex and concave curvatures and adverse pressure gradient. *Experiments in Fluids*, 31:697–707.

Webster, D. R., DeGraaff, D. B., and Eaton, J. K. (1996). Turbulence characteristics of a boundary layer on a two-dimensional bump. *Journal of Fluid Mechanics*, 320:53–69.

Wu, X. and Squires, K. D. (1998). Numerical investigation of the turbulent boundary layer over a bump. *Journal of Fluid Mechanics*, 362:229–271.

Zagarola, M. V. and Smits, A. J. (1998). A new mean velocity scaling for turbulent boundary layers. *ASME Fluids Engineering Division Summer Meeting June 21-25, Washington DC*, FEDSM98-4950.